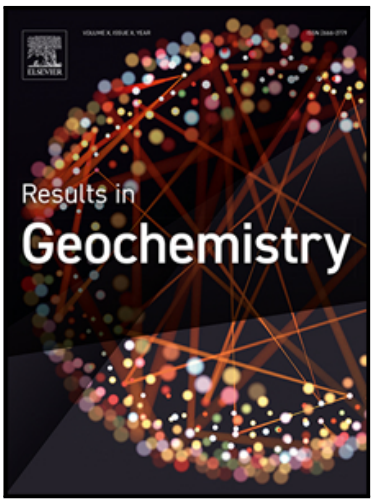

Condensation corrosion alters the oxygen and carbon isotope ratios of speleothem and limestone surfaces

Jackson H. White , David Domínguez-Villar , Adam Hartland

PII: S2666-2779(21)00001-0
DOI: https://doi.org/10.1016/j.ringeo.2021.100008
Reference: RINGEO 100008

To appear in: *Results in Geochemistry*

Received date: 21 July 2020
Revised date: 9 February 2021
Accepted date: 16 February 2021

Please cite this article as: Jackson H. White , David Domínguez-Villar , Adam Hartland , Condensation corrosion alters the oxygen and carbon isotope ratios of speleothem and limestone surfaces, *Results in Geochemistry* (2021), doi: https://doi.org/10.1016/j.ringeo.2021.100008

Highlights

- Condensation corrosion is detected using stable isotope analysis of calcite surfaces
- Dissolution and recrystallization cause distinct changes in C and O isotope ratios
- Negative isotope correlation from degassing (higher $\delta^{13}C$) and condensation (lower $\delta^{18}O$)
- Results are consistent with high-resolution studies of speleothem hiatuses
- A new approach to the detection of condensation corrosion in managed caves

Condensation corrosion alters the oxygen and carbon isotope ratios of speleothem and limestone surfaces

Jackson H. White[a], David Domínguez-Villar[b], Adam Hartland[a,*]

[a]Environmental Research Institute, School of Science, Faculty of Science and Engineering, University of Waikato, Hamilton, New Zealand

[b]Department of Soil Science, Faculty of Agriculture, University of Zagreb, Svetošimunska 25, 10000, Zagreb, Croatia

* Corresponding author: adam.hartland@waikato.ac.nz

Abstract

Condensation corrosion is a natural process which enhances the chemical weathering of limestone cave chambers and speleothems. We evaluated the use of carbonate tablets for detecting condensation corrosion in Glowworm Cave, New Zealand, using local limestone and speleothem as experimental substrates (herein tablets). Evidence for condensation corrosion was assessed via three methods: gravimetric (mass wasting), microscopic (surface pitting, recrystallization) and isotopic ($\delta^{13}C$ and $\delta^{18}O$ changes). Our results show little evidence of tablet mass loss throughout a 6-month deployment period. However, SEM imaging and isotope analysis ($\delta^{13}C$ and $\delta^{18}O$) of the upper ~50 µm layer of the tablets, suggest that condensation corrosion operates in the cave, especially in sectors affected by large diurnal microclimate variations.

Most notably, condensation water altered the tablet surface $\delta^{13}C$ and $\delta^{18}O$ values. Small, positive shifts in surface $\delta^{13}C$ and $\delta^{18}O$ values are considered to reflect pure dissolution (where dissolution favours the removal of lighter isotopologues). In contrast, tablets that exhibited large positive shifts in $\delta^{13}C$ in tandem with large negative shifts in $\delta^{18}O$ values, are interpreted as showing calcite recrystallization and the inheritance of higher DIC $\delta^{13}C$ values (^{13}C fractionation by CO_2 degassing), lighter water $\delta^{18}O$ values and/or kinetic fractionation of $\delta^{18}O$. This study therefore demonstrates that stable isotopes could be applied to detect paleoclimatic episodes of condensation corrosion in speleothems.

Keywords:

Isotope fractionation; recrystallization; speleothem; Paleoclimate; hiatus; cave management

Graphical abstract

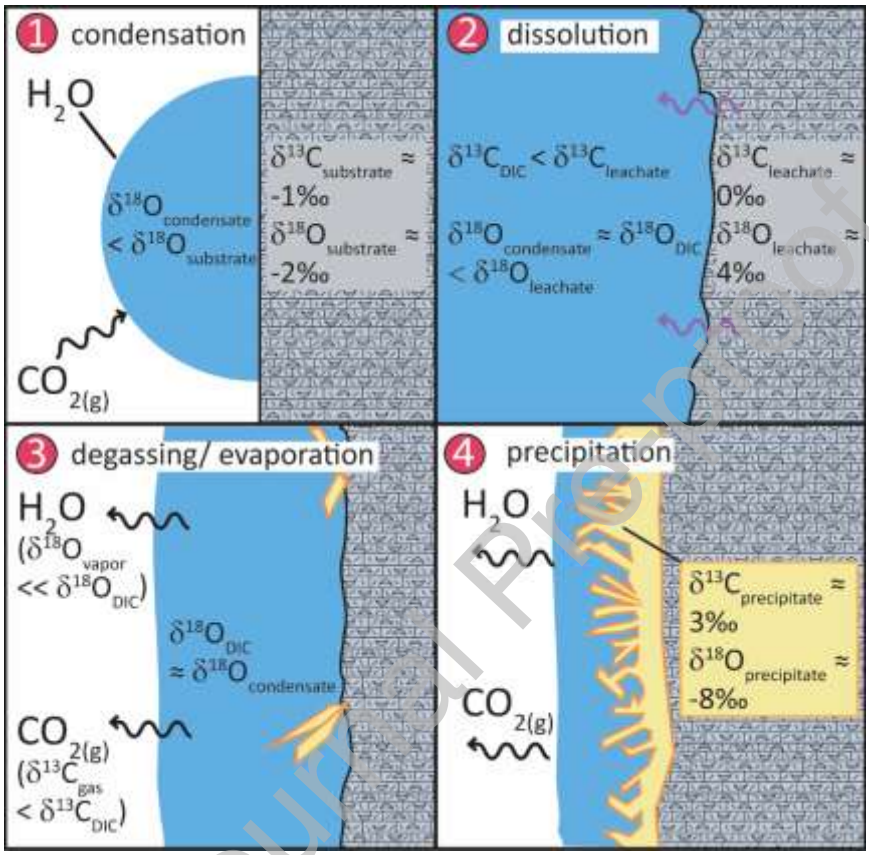

1. Introduction

Condensation corrosion is a chemical weathering process that enlarges limestone cave chambers through the dissolution of walls covered in condensation (Figure 1) [1-3]. Condensation corrosion occurs when $CaCO_3$ dissolves due to the action of atmospheric CO_2 diffusing into a water film on the bedrock surface [2,4]. This process also occurs in gypsum caves ($CaSO_4 \cdot 2H_2O$), where it is known as condensation-solution [5], resulting in gypsum dissolution. In heavily trafficked tourist caves, condensation corrosion can potentially accelerate the degradation of cave formations, and cave art in some cases, because of more extreme microclimate variability.

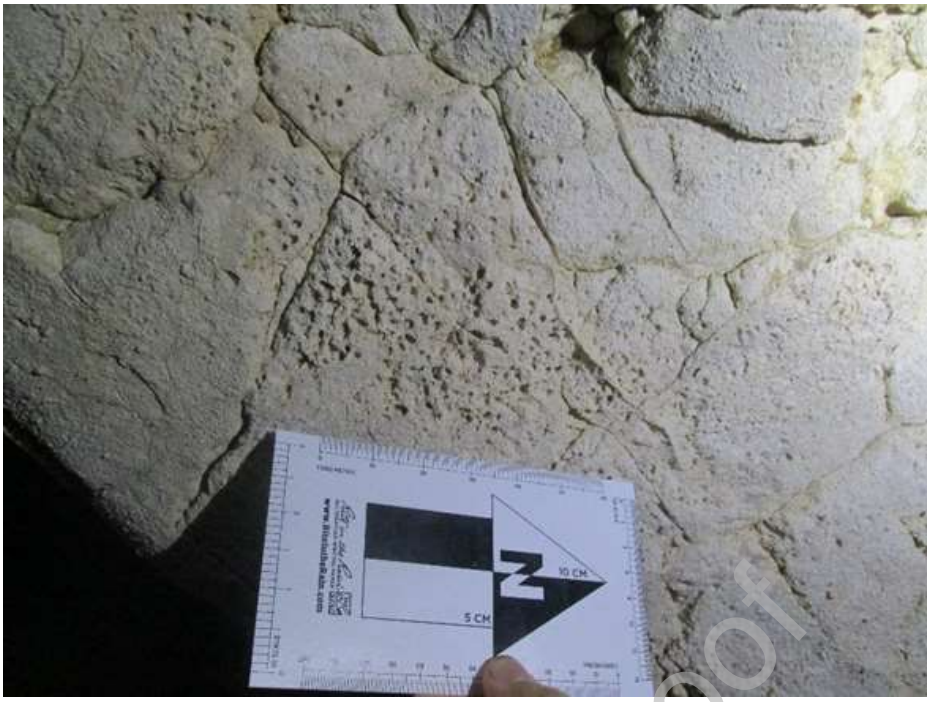

Figure 1: Condensation corrosion dissolution features on the limestone ceiling in Tomo Passage, Waitomo Glowworm Cave. Photo from Ingrid Lindeman.

The Waitomo Caves, including Glowworm Cave, attracted over half a million tourists in 2016 and generated $71 million New Zealand dollars [6]. Tourism in these caves causes major changes in cave air temperature, relative humidity and CO_2 concentration, with potential to increase the rate of condensation corrosion. This is of concern because tourism has resulted in permanent deterioration of speleothems in other settings [7]. While the importance of condensation corrosion in each setting will vary with the local conservation values, it is important to understand how tourism may impact cave microclimate, cave formations and ecosystems. [8]

Previous studies in the Glowworm Cave have focused on conservation of cave formations through understanding cave air pCO_2 dynamics, including examination of the non-anthropogenic sources of carbon dioxide (CO_2) (i.e. stream pCO_2) [9] and chamber microclimate and ventilation [10]. In this study, we investigated condensation corrosion [8] with the aim of developing an empirical method to detect condensation corrosion in a cave setting where the ongoing impacts of visitation are ambiguous.

1.1 Geochemistry of condensation corrosion

The condensation corrosion process begins from dew deposition as a thin film on cave walls. Cave walls can be composed of a mix of soluble minerals such as calcite, dolomite, halite or gypsum. Dissolution of these minerals then occurs at the interface between the condensation water and rock surface [2]. The dissolution rate depends on the amount of condensation water on the rock surface over time and the concentration of atmospheric CO_2 [11]. The temperature gradient between the condensation water and rock surface only plays a minor role in corroding the rock surface, since the condensation water rapidly reaches thermal equilibrium. Condensation water becomes corrosive when CO_2 diffuses from the atmosphere into the water droplets, or water film (equation 1) forming carbonic acid (equation 2). Carbonic acid can dissociate by the reactions shown in equations 3 and 4 depending on the temperature, thereby changing the pH of the water [2].

$$CO_{2_{(g)}} \rightleftharpoons CO_{2_{(aq)}} \quad (1)$$

$$CO_{2_{(aq)}} + H_2O \rightleftharpoons {H_2CO_3}^0_{(aq)} \quad (2)$$

$${H_2CO_3}^0_{(aq)} \rightleftharpoons H^+_{(aq)} + {HCO_3}^-_{(aq)} \quad (3)$$

$${HCO_3}^-_{(aq)} \rightleftharpoons H^+_{(aq)} + {CO_3}^{2-}_{(aq)} \quad (4)$$

The sum of all carbonate species in solution is known as dissolved inorganic carbon (DIC). DIC is largely composed of HCO_3^- at pH values typical of limestone caves [12].

1.2 Phase change and isotope exchange

Cave climate is responsive to the thermodynamic interaction between external air and cave air [13]. These interactions result in changes in condensation and evaporation rates. Condensation takes place when the air temperature decreasesand condensate forms on cooler surfaces, such as cave walls and speleothems. Evaporation is the opposite process and occurs when the cave air increases in temperature leading to a condensate losing water to the atmosphere [14,15].

1.2.1 Condensation

In caves, condensation occurs because of the sudden temperature change at the interface of the cave wall and air [16]. Initially, the wall temperature increases due to the latent heat release from the water vapour. During the deposition of condensation, atmospheric CO_2 dissolves into the condensation water lowering the pH and dissolving some $CaCO_3$. If the atmospheric CO_2 concentration lowers, or relative humidity drops, then CO_2 in the condensation water will degas, causing calcite precipitation. During the lifetime of a condensation film, dissolution and possible grain detachment of less-soluble bedrock caused by dissolution may also occur. Features of these processes were observed in our initial surveys of the Tomo Passage, Glowworm Cave (Figure 1); a proposed mechanism of formation is illustrated in Figure 2. Note the microcrystalline calcite depicted in the photograph (Figure 1) can formed by condensation, re-evaporation cycles, or by evaporation of water flowing along the seepage network. Microcrystalline calcite has been observed around the world in different cave climates, carbonate lithologies [16,19-25], and sulphate lithologies [5,26-28].

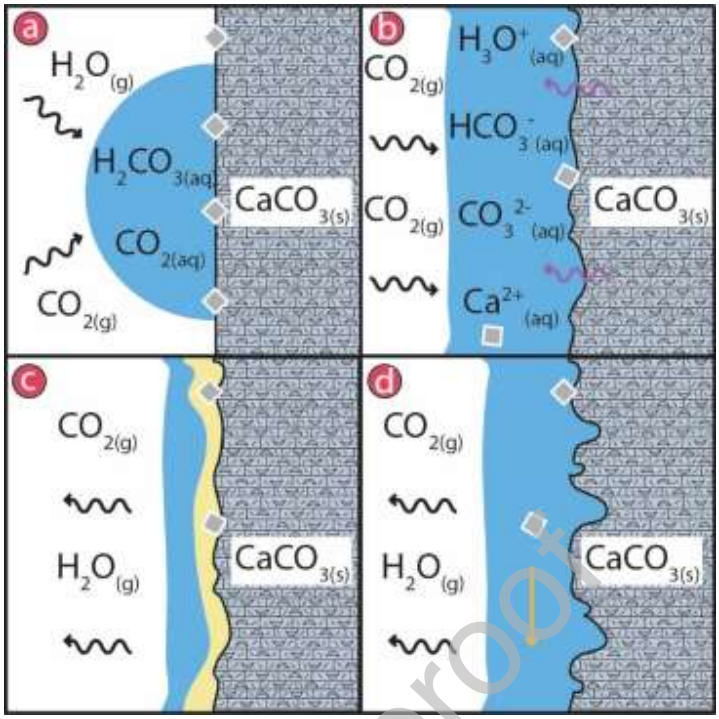

Figure 2: Formation of microcrystalline calcite. a) The formation of microcrystaline calcite begins with the nucleation of water on the cave wall surface and subsequent diffusion of atmospheric CO_2 into the condensate ($CO_{2(aq)}$). $CO_{2(aq)}$ hydrates forming carbonic acid ($H_2CO_{3(aq)}$). b) $H_2CO_{3(aq)}$ then dissociates releasing H^+, which instantly forms hydroxonium ions ($H_3O^+_{(aq)}$). $H_3O^+_{(aq)}$ enhances limestone dissolution (purple arrows), ionizing the calcite components into $Ca^{2+}_{(aq)}$ and $CO_3^{2-}{}_{(aq)}$, and releasing less soluble grains from the bedrock (grey diamonds). All ions in solution will move along with the water film. Removal of the more-soluble matrix will loosen less-soluble grains, which eventually detach from the cave wall. Grain detachment is the mechanism where most of the mass is lost from the cave wall. c) When evaporation of condensate takes place, the solution supersaturates leading to the precipitation of microcrystaline calcite (yellow layer). d) However, if the water flows down the wall (orange arrow representing the direction of flow), the bulk mass transport of the dissolved ions will result in dissolution features as those of (Figure 1).

1.2.2 Evaporation

Evaporation takes place when the relative humidity is less than 100%, and the atmosphere is undersaturated in water vapour. Evaporation is considered a kinetic process [30,31], where the lighter H_2O isotopologues preferentially evaporate from solution. Likewise lighter $CO_{2(g)}$ molecules degas [32,33] in response to a lowering of CO_2 partial pressure of the cave atmosphere (typical of touristic caves). Therefore, the residual heavier isotopologues of H_2O and CO_2 accumulate in solution resulting in exchange of heavier isotopes between H_2O, CO_2 and the DIC species. Calcite precipitated under these conditions is expected to have more positive $\delta^{13}C$ values

[20,32-35]. However, heavier (more positive) $\delta^{18}O$ values may not be identified due to the "buffering" effect caused by the much greater abundance of H_2O (relative to DIC) in solution [36,37]. It can be the case that evaporation of H_2O can lead to high $\delta^{13}C$ and $\delta^{18}O$ values in precipitated calcite (Deininger *et al.*, (2012)), when relative humidity is sufficiently low and wind velocity is high. Deininger *et al.*, (2012) concluded that high evaporation rates are conducive to high calcite precipitation rates, because of the increased concentration of Ca^{2+} and HCO_3^-.

2. Study site

The Waitomo Glowworm Cave is located at latitude 38°15'S and longitude 175°06'E; in Waitomo, New Zealand, in a temperate oceanic climate (Köppen climate classification). The cave is located in the northeast-trending Waipa Fault [38,39], which focusses water flow under the karst landscape. The cave is developed in Otorohanga Limestone, a shallow marine grain-dominated packstone formed between 37.8 and 28.1 million years ago. [40].

2.1. Study locations within Glowworm Cave

The Glowworm Cave consists of 1300 m of interconnected passageways and has an estimated volume of 4000 m^3 [1]. The cave has an upper and a lower entrance, which are 14 m apart vertically and its main passage is 39 m long with an elliptical cross-section varying between 3-7 m^2 [1]. The Waitomo Stream passes through the lower entrance of the cave. Five sites were selected to study the effects of corrosion on tablets: the Upper Entrance, the Blanket Chamber, Tomo Passage, Organ Loft and Cathedral Chamber (Figure 3). Microcrystalline calcite is common on the cave walls and speleothem of the Blanket Chamber, lower parts of the Cathedral Chamber and speleothem in the Entrance Chamber. In contrast, the Tomo Passage and Organ Loft had very little of this texture present which is confined to fractures in the bedrock.

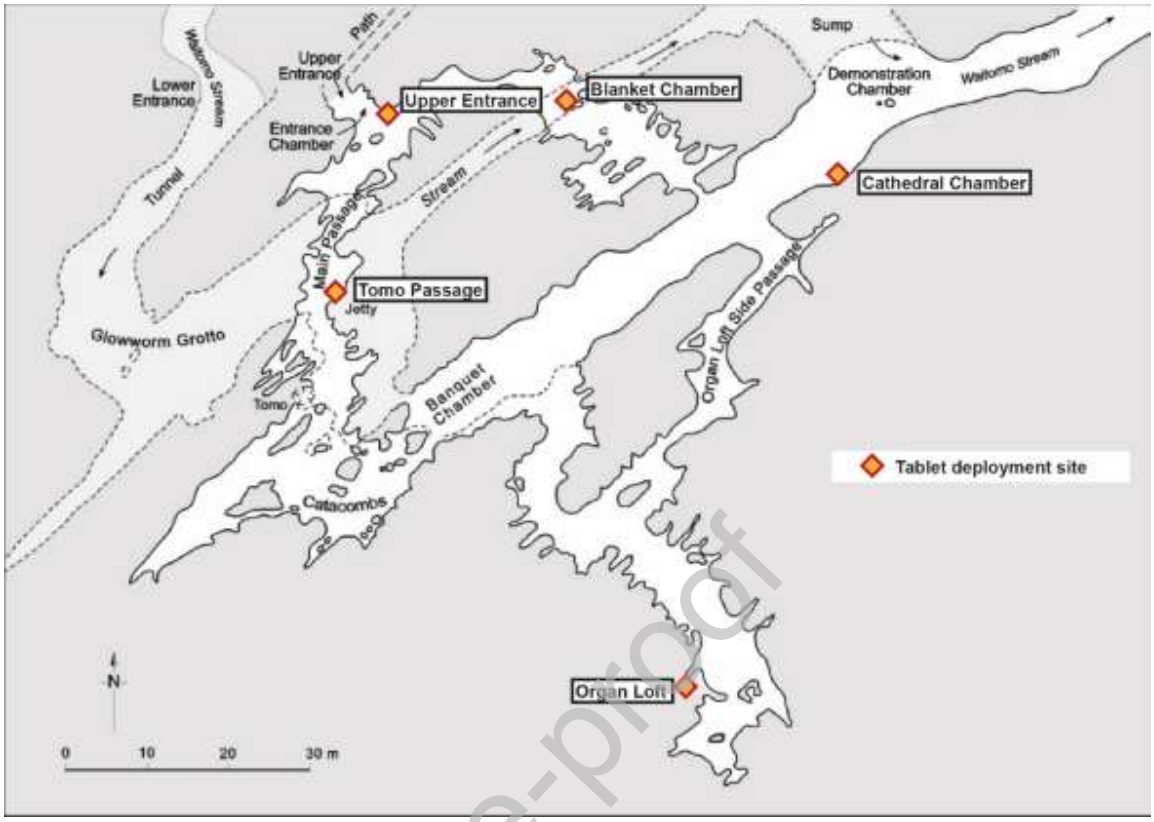

Figure 3: Glowworm Cave map modified from de Freitas and Schmekal [1] showing the tablet deployment sites and de Freitas and Schmekal [1] condensation measurement sites. The upper part of the cave is marked by the solid black line and the lower passages are indicated by a dashed line.

3. Methods

3.1 Tablet method

The tablet method consists of the installation of a previously weighed rock specimen composed of the local bedrock or speleothem onto the cave wall. By evaluating the mass difference following the recovery of the tablet, the mass loss due to condensation corrosion is determined.

The Glowworm Cave bedrock is composed of Otorohanga Limestone, from which the limestone tablets were sourced. The speleothem tablets were sourced from a stalactite sample from Waipuna Cave, Waitomo, also developed in Otorohanga Limestone. The limestone samples were taken from the unweathered interior of a limestone boulder taken from the vicinity of the Glowworm Cave. At each site, 32 tablets of limestone and 32 tablets of speleothem were deployed. After four

months, 16 tablets of the limestone and 16 of the speleothem tablets were removed per site. After six months, the rest of the tablets were collected.

Both limestone and speleothem tablets were cut using a rock saw, producing plate-shaped tablets with sides of approx. 20 mm length and thicknesses of approx. 4 mm (Figure 4). Because the rock saw is designed to cut rock cores and not prismatic shapes, the sides were made as close as possible to being perpendicular, but there was some variability in length due to the thickness of the saw blade.

The samples were later polished using a grinding-polishing machine for making thin sections. The sandpaper used was made of silicon carbide with 500 grit (30.2 µm in diameter). The tablets were then immersed in a deionized water ultrasonic bath for 3 minutes, then placed into an oven for 24 hours at 50°C and allowed to cool in a desiccator for 2 hours. The tablets were weighed once with a four decimal place balance and stored in individual zipper-lock bags with most of the contained air removed. When the tablets were deployed, they were emplaced using a silicone sealant. By attaching the tablets to the cave wall we assumed that the tablet temperature would equilibrate with the cave wall instead of cave air. Otherwise, if the tablet equilibrated with the cave's atmosphere, condensation would eventually cease and our results would not be reflective of that of the cave wall.

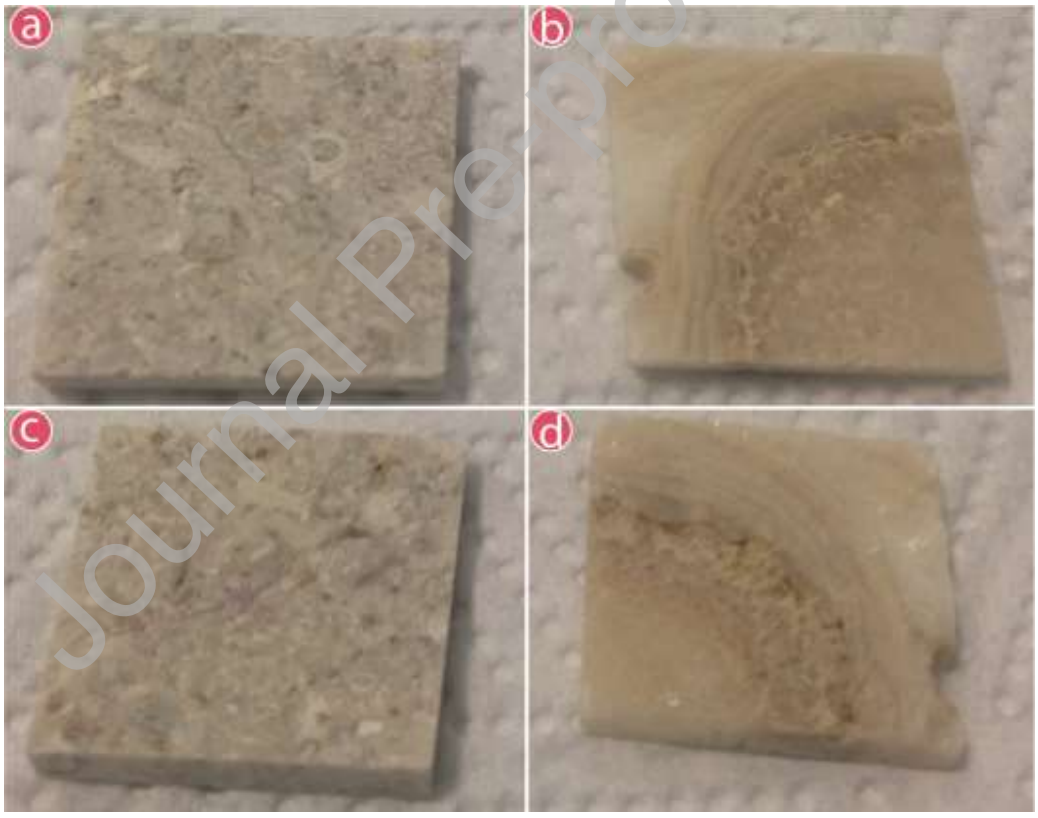

Figure 4: Examples of limestone and speleothem tablets. (a) and (b) show the exposed sides of a limestone and speleothem tablet, respectively. (c) and (d) are the glued side of the tablets in (a) and (b). Tablets made of speleothem typically have larger pores than their bedrock limestone counterparts.

When the samples were collected, they were sealed in individual zip-lock bags with most of the interior air removed. The samples were later cleaned using damp

earbuds, the silicone was removed, and the tablets were placed in an ultrasonic bath for 3 minutes, placed in an oven for 24 hours at 50°C and left to cool in a desiccator for 2 hours before being reweighed.

Limestone and speleothem tablets (Figure 4) were deployed at different sites in the Glowworm Cave on the 9th of March, 2018 and retrieved over two stages. Stage one lasted about four months (samples retrieved on the 28th of June, 2018) and stage two lasted about six months (samples retrieved on the 31st of August, 2018). The exposed surfaces were later analysed for condensation corrosion features using scanning electron microscopy (SEM) and the tablets were reweighed using the aforementioned protocol. Deployed tablets (and tablet blanks) were thus characterized gravimetrically, mineralogically and isotopically.

3.2 X-ray powder diffraction (XRD)

XRD was used to characterise the mineral composition of the cave bedrock and stalactite both used in making the tablets. The instrument used was a Panalytical Empyrean XRD Series 2, in X-Ray Diffraction and Fluorescence lab at The University of Waikato. Samples were crushed to a fine powder using a tungsten-carbide ring-mill and analysed in the 20-40°2θ range at 50 seconds per step.

3.3 X-ray fluorescence (XRF)

XRF was used to characterize the elemental composition of tablet substrates [41]. A Brunker S8 Tiger wavelength dispersive X-ray spectrometer with a detection limit for CaO of 35.5 ppm was used. Samples were dried and homogenized by being made into powders and then fused into disks for major elements.CO_2 was calculated by mass difference after loss on ignition (LOI) of the sample at 1100 °C, to a precision of ± 0.1 mg.

3.4 Microclimate monitoring

Air temperature variations were recorded at different sites using Hobo tidbit (Onset Computer Corp, Bourne, MA, USA) data loggers. The data loggers were glued with silicone adhesive to the cave walls to record tablet-specific temperature changes

with a 1-minute logging frequency and a stated accuracy of ±0.21°C. The loggers were deployed for 6 months, at the same time as the tablets. Other reported cave climate data have been provided by the cave management company, Tourism Holdings Ltd.

3.5 Scanning Electron Microscopy (SEM)

SEM was used to identify micromorphological features of corrosion and precipitation of calcium carbonate crystals. The tablets were prepared following the procedure in [42]. Imaged tablets were coated in platinum for 80 seconds using a Hitachi E1030 Ion Sputter Coater. The platinum coated samples had a double-sided carbon tape placed along the middle of the face that had been attached to the cave wall. These samples were then mounted onto aluminium stubs using carbon tape. One edge of the double-sided tape was coated using ProSciTech water-based carbon/graphite adhesive, ensuring it was in contact with the tablet surface and aluminium stub. SEM images were taken using a Hitachi S-4700 cold field emission microscope set at 5kV and 15 kV. EDS analysis confirmed the composition of $CaCO_3$ precipitates, where present.

3.6 Isotope analysis

$\delta^{13}C$ and $\delta^{18}O$ values were determined in sample aliquots of the tablets before and after exposure to assess whether the tablet surfaces had undergone dissolution and/or precipitation as a result of condensation and evaporation processes. The $\delta^{13}C$ and $\delta^{18}O$ values were measured in calcite sub-samples milled from the upper surface of the tablets deployed in the Blanket Chamber and Tomo Passage. Surfaces were milled to ca. 50 μm depth to characterise the upper layer of material which has the greatest potential for alteration by corrosion. The Blanket chamber and Tomo Passage were selected for isotope analysis as tablets from these locations more frequently showed *clear precipitation of calcium carbonate under SEM*. The tablet data was compared to unaltered limestone and speleothem samples, as well as to the microcrystalline calcite sample from the Blanket chamber. The isotope analysis was achieved by using a continuous flow method [43], which involves pumping the

laboratory atmosphere (also used for drift correction) through a Drierite column to produce a zero CO_2 gas. This treated gas carries the CO_2 sample from the vials into the optical cavity of a Los Gatos Research CCIA-48 Carbon and Oxygen Isotope Analyzer. This instrument was calibrated using external reference materials NBS 19 (limestone, IAEA), Sigma (synthetic carbonate) and BDH (synthetic carbonate) [44]. Table 1 shows the standard deviation of the external reference materials between and across runs, in which an average sample mass of 2.12 ± 0.1 mg was used.

Table 1: Standard deviation of external standard between and across runs

Run	**Reference material**	**$\sigma_{\delta 13C}$ (‰)**	**$\sigma_{\delta 18O}$ (‰)**	**Sample size**
1	NBS19	2.3	0.2	4
	Sigma	0.9	2.7	4
	BDH	1.1	3.4	4
2	NBS19	0.1	0.2	2
	Sigma	0.1	0.7	2
	BDH	0.1	3.4	2
3	NBS19	0.2	1.0	3
	Sigma	0.3	0.5	3
	BDH	0.3	0.7	3
Mean σ between runs	NBS19	0.9	0.5	9
	Sigma	0.4	1.3	9
	BDH	0.5	1.4	9

Variability across runs	NBS19	1.7	1.7	10
	Sigma	0.7	1.8	10
	BDH	0.7	2.0	10

3.7 T-test (t-statistic)

The t-test was used to compare the average weight change difference between the initial and final speleothem tablets and limestone tablets as well as the change in the surface $\delta^{13}C$ and $\delta^{18}O$ composition of the tablets. We were interested in observing any average weight differences as this is fundamental evidence of condensation corrosion in action. A comparison of the $\delta^{13}C$ or $\delta^{18}O$ composition of tablets before and after exposure was also considered as a means of identifying reactions taking place on the tablet's surface that might be otherwise difficult to detect. Therefore, the t-test was used to assess opposing hypotheses in regards to the means of the initial and final sets [45].

Typically, if two means are separated by more than two standard deviations (σ), they are statistically different [46]. The t-statistic (t) is computed by equation (5):

$$t = \frac{\bar{x}_1 - \bar{x}_2}{\sqrt{\frac{{\sigma_1}^2}{n_1} + \frac{{\sigma_2}^2}{n_2}}} \quad (5)$$

where $\bar{x}_1$ and $\bar{x}_2$ are the sample mean of each group; σ_1 and σ_2 are their respective sample standard deviations; and n_1 and n_2 are their respective sample sizes [46]. The null hypothesis (H_0) is when there is less than 2σ between means, and is interpreted as no statistical difference between the means; while the alternative hypothesis (H_a) is statistically different between both means [47].

4. Results

4.1 Tablet mass deviations

XRF results show that the Otorohanga Limestone and Waipuna speleothem used in the tablet making was composed of 97% and 99% calcium carbonate, respectively; while the XRD demonstrated that both materials were mostly calcite. Gravimetric results were analysed using a t-test to first determine whether this method produced meaningful results. To do so our null hypothesis was defined as "there was no difference in the average mass change between initial and final tablet weight". The sample means, standard deviation and sample size for the limestone and speleothem tablet groups can be found in Table 2. The level of significance in this t-test was 0.05, and a 95% confidence interval was applied to both sets. No statistically significant change was found in either the limestone or speleothem tablets.

Table 2: Statistical parameters used to evaluate whether there was a difference in mass change between initial and final weight in limestone and speleothem tablets.

Tablet	Mean (g)	Sample Standard deviation (g)	Sample size
Initial limestone	2.768	0.618	74
Final limestone	2.767	0.618	74
Initial speleothem	2.873	0.864	70
Final speleothem	2.869	0.863	70

4.2 Microclimate characterisation using air temperature loggers

Temperature data were used to compare the microclimate between sites (Figure 5a). Air temperature varied most in the Upper Entrance, Tomo Passage and Cathedral Chamber, in contrast to the more stable temperatures of the Blanket Chamber and Organ Loft. This largely reflects the proximity of sites relative to the main ventilation source but also captures the effects of tourist groups during visitation hours. Because visitation of Glowworm Cave is a daytime activity, cave

temperature variations due to tourists are also coupled to dynamic changes in atmospheric pCO_2 (varying between 441.1 and 2365 ppmv in April 2018) and relative humidity, with both these variables being expected to drive diurnal fluxes of CO_2 and H_2O between cave air and tablet surfaces (Figure 5b).

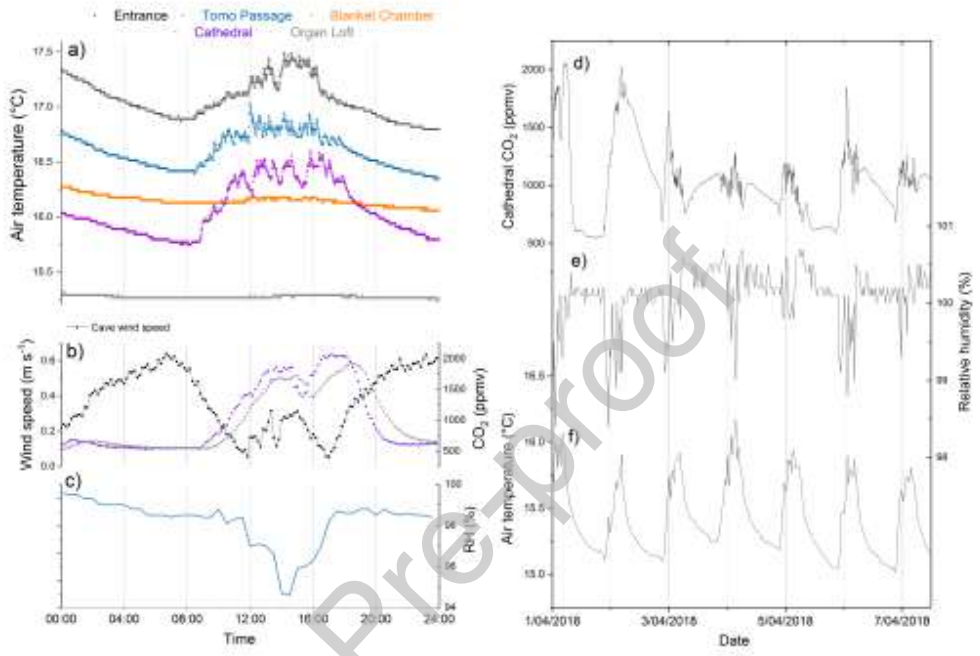

Figure 5: (a) Temperature variation in the Upper Entrance, Tomo Passage, Blanket Chamber and Organ Loft over 24 hrs on 1st April 2018. (b) Logger data from the same 24 hour period including cave wind and PCO_2, Cathedral Chamber (purple dots) and Organ Loft (grey dots). (c) Tomo Passage relative humidity (RH). Diurnal fluctuations in microclimate variables are caused by the presence/absence of tourist groups and ventilation by the opening of the entrance door. Panels (d), (e) and (f) show the daily variation of *P*CO2, RH and air temperature, over a week (1st of April, 2018 to the 7th of April, 2018).

4.3 SEM characterisation of tablet surfaces

Dissolution and crystallization features were not observed frequently under SEM. However, Figure 6 shows some evidence of corrosion, and Figure 7 can be used as a reference for tablets before exposure. Figure 6a shows a limestone tablet exposed for four months in the Cathedral Chamber, where the tablet has pitting on calcite crystals. Figure 6b shows a cluster of dissolution features on the surface of a 6-month exposed limestone tablet from the Tomo Passage. Figure 6c shows precipitation of newly formed calcium carbonate crystals (confirmed by EDS

analysis). These features were deposited on top of a limestone tablet during four months of exposure in the Blanket Chamber. Figure 6d shows calcite precipitation with lineal dissolution features. Fungi were found on tablets after collection. These were cultivated in agar plates and identified under light microscopy as *Aspergillus* sp., *Penicillium* sp., *Cladosporium* sp., *Rhizopus* sp.

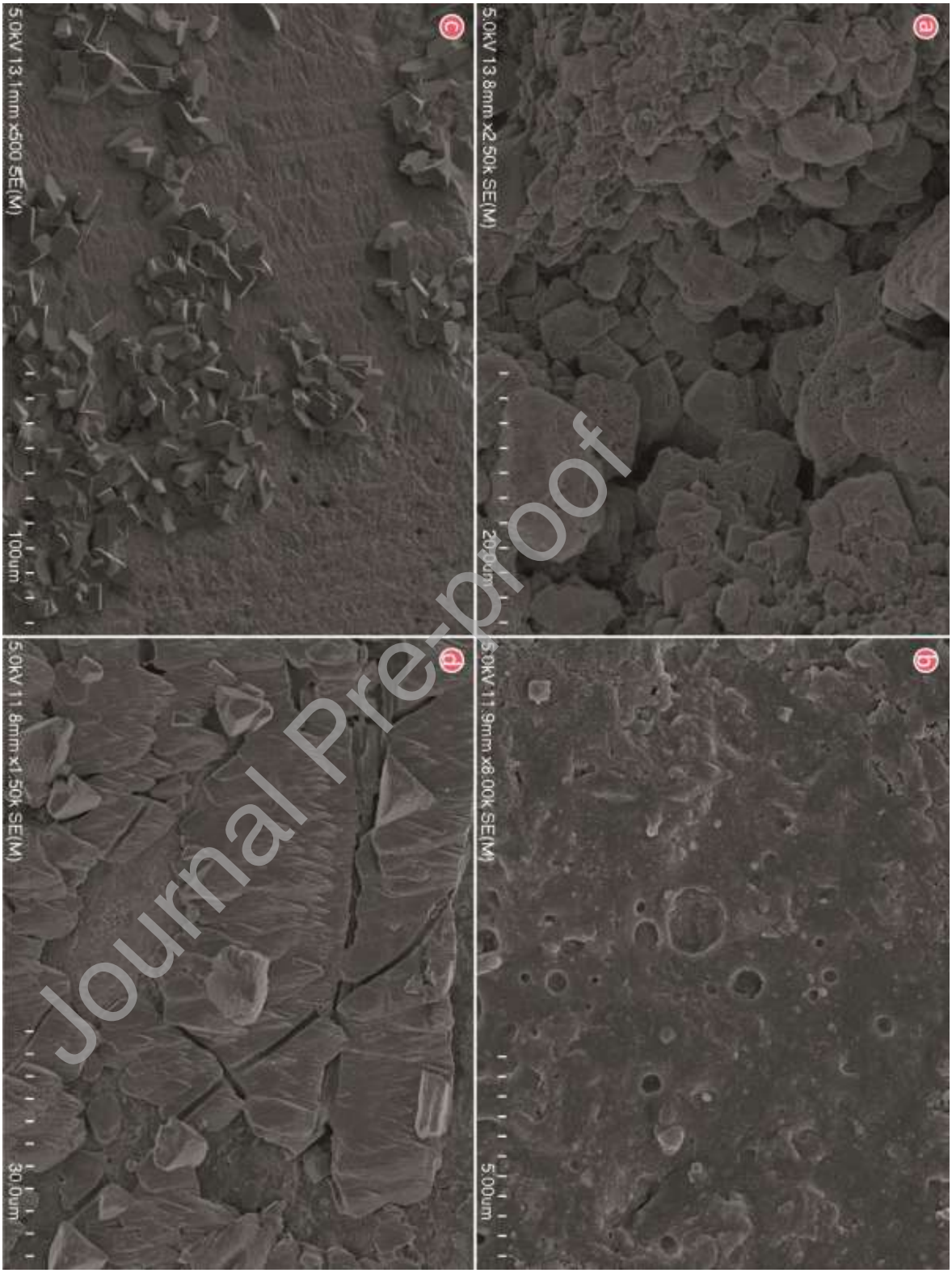

Figure 6: SEM images from tablets exposed to the Glowworm Cave environment (a) Pitting into calcite crystals of a limestone tablet from the Cathedral Chamber after four months of exposure. (b) Dissolution features found on a limestone tablet after six months of exposure in the Tomo Passage. (c) Calcium carbonate crystallization on limestone tablet from the after six months of exposure to the

Blanket Chamber. (d) Linear dissolution features on precipitated crystals after 3 months in the Tomo Passage.

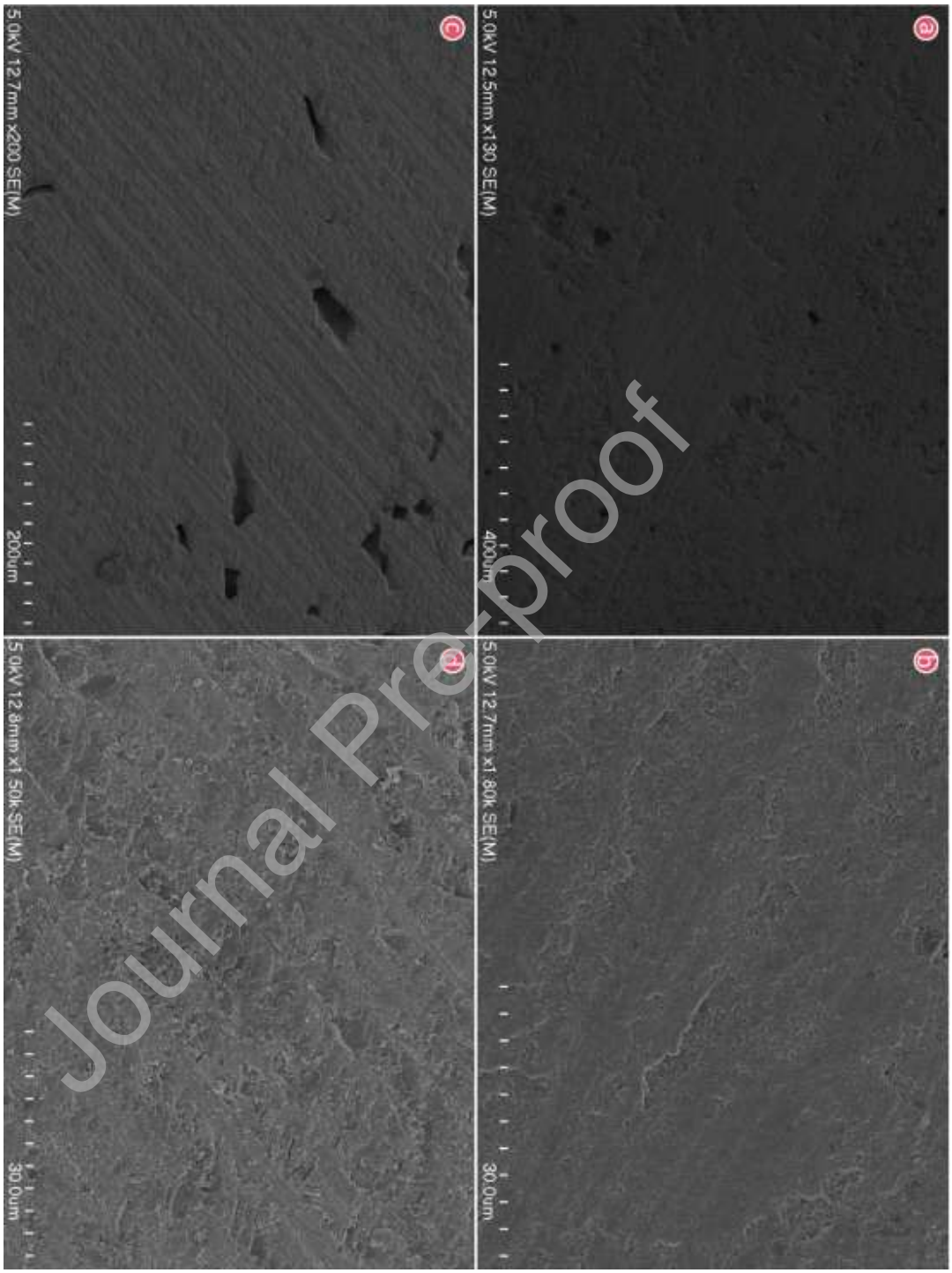

Figure 7: Tablet surfaces before exposure. (a) and (b) show the surface of a limestone tablet at a 400 µm and 30 µm scale, respectively. (c) and (d) show the surface of a speleothem tablet at a 200 µm ad 30 µm scale.

4.4 $\delta^{13}C$ and $\delta^{18}O$ values of exposed and unaltered substrates

The unaltered limestone and speleothem tablets occupied distinct regions of $\delta^{18}O$ and $\delta^{13}C$ space (Figure 8). The Otorohanga Limestone bedrock was characterised by mean $\delta^{18}O$ and $\delta^{13}C$ values of -2.1 and -1.5 ‰ VPDB. A similar, but a tighter range of values was found for the microcrystalline calcite sample ($\delta^{18}O$ and $\delta^{13}C$ mean values of -2.7 and -1.0 ‰ VPDB). In contrast, the speleothem tablets had tightly correlated $\delta^{18}O$ and $\delta^{13}C$ mean values of -5.2 and -8.7 ‰ VPDB, consistent with a greater contribution of C_3 biogenic carbon inputs [48] and kinetic fractionation during speleothem deposition. This distinction between initial isotope compositions of the limestone and speleothem, and the tight clustering of speleothem values prove useful in subsequent analysis and rationalisations.

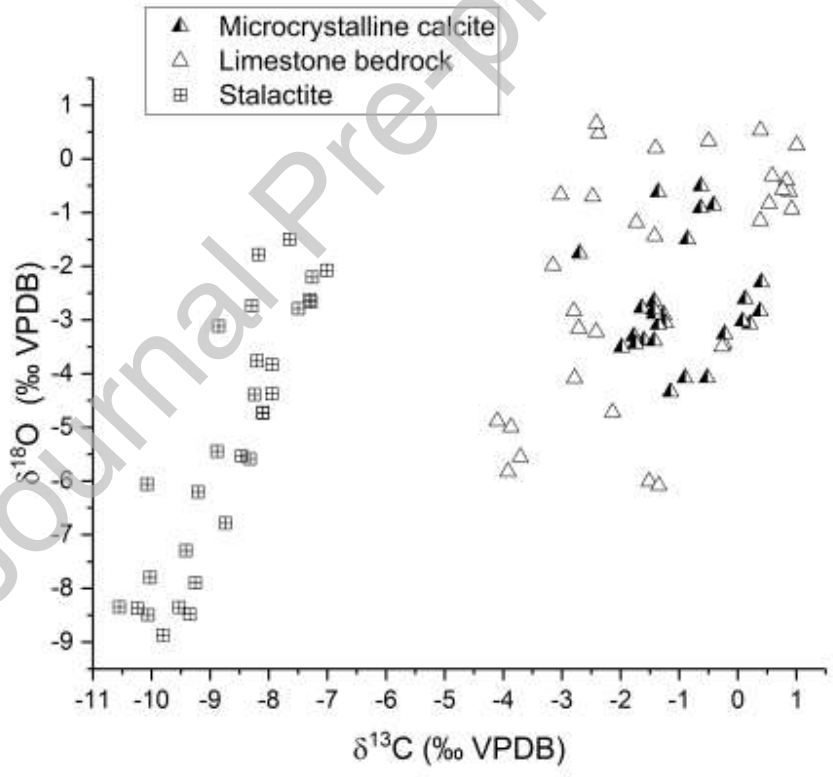

Figure 8: Carbonate $\delta^{18}O$ and $\delta^{13}C$ values for the materials used as tablet substrates (limestone and speleothem) and microcrystalline calcite.

Normal distribution curves were computed for speleothem and limestone tablet $\delta^{13}C$ values (Figure 9a) and $\delta^{18}O$ values (Figure 9b). These curves were compared to unaltered limestone, unaltered speleothem, and microcrystalline calcite samples. $\delta^{13}C$ normal distribution curves have smaller ranges which do not overlap as much as those from the $\delta^{18}O$ curves. The sample mean, sample standard deviation and sample number of each set are given in Table 3.

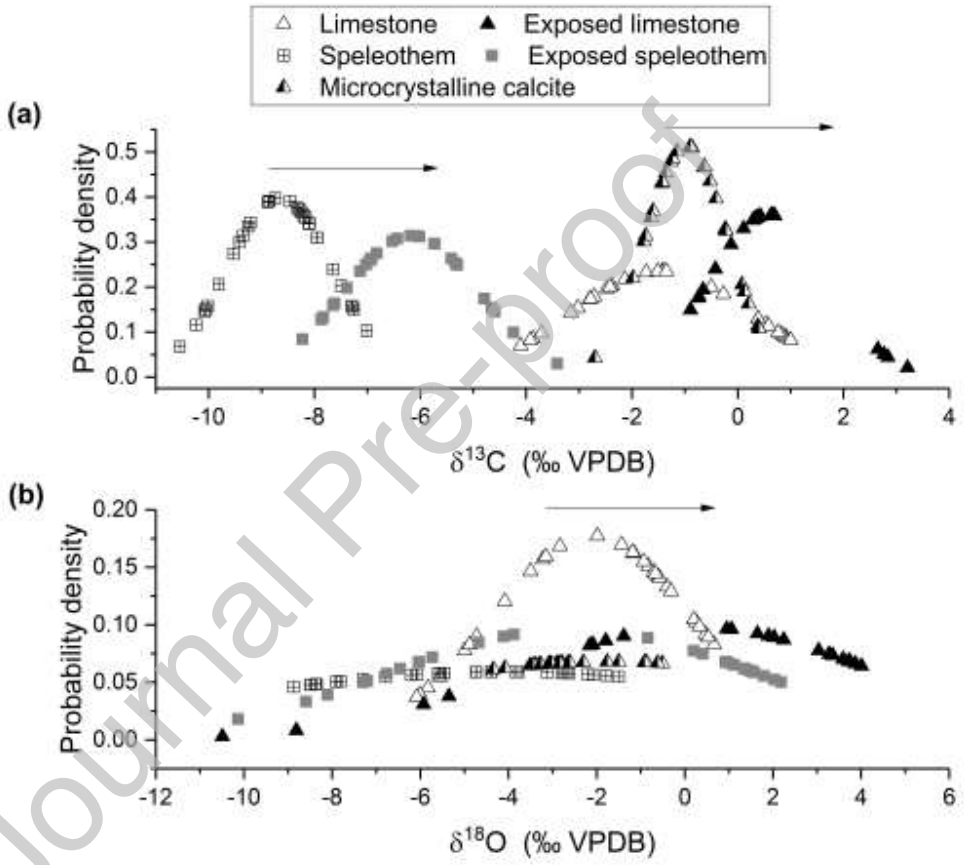

Figure 9: Normal distribution curves of (a) $\delta^{13}C$ and (b) $\delta^{18}O$ values of unaltered and exposed tablets in addition to microcrystalline calcite. The direction of the shift in population means (calcite dissolution/precipitation) is shown by the arrows. The clearest change is seen in $\delta^{13}C$.

Table 3: Sample mean ($\bar{x}$) and sample standard deviation (σ) of $\delta^{13}C$ and $\delta^{18}O$ of exposed tablets and unaltered speleothem and limestone. n is the sample size.

	δ^{13}C (‰)			δ^{18}O (‰)		
Statistic	$\bar{x}$	σ	n	$\bar{x}$	σ	n
Exposed speleothem tablets	-6.2	1.3	27	-2.6	4.1	27

Unaltered speleothem samples	-8.7	1.0	30	-4.1	6.8	30
Exposed limestone tablets	0.6	1.1	26	0.3	4.1	26
Unaltered limestone samples	-1.5	1.7	30	-2.1	2.3	30
Microcrystalline calcite samples	-1.0	0.8	29	-1.7	5.9	29

Table 4 shows the $\delta^{18}O$ and the $\delta^{13}C$ differences between the means of experimental sets. The differences were analysed using a t-test since the statistical requirements are also met by this data set. The null hypothesis (H_0) was that no observable change was computed between the unaltered and altered materials. Therefore, the alternative hypothesis (H_a) states that there was a change between materials. The four data sets accepted the alternative hypothesis, favouring a statistically significant difference between the altered and pristine materials concerning $\delta^{18}O$ and $\delta^{13}C$ values.

Table 4; Calculations for t-test comparing $\delta^{18}O$ and $\delta^{13}C$ values of limestone and speleothem. ($\overline{x}_1 - \overline{x}_0$) represents the sample mean difference between the exposed sample, $\overline{x}_1$, and the unaltered sample, $\overline{x}_0$. A "H_a" (alternative hypothesis) was assigned to the columns where a statistical difference between the means is accepted. Otherwise, instead of a "H_a", an "H_0" (null hypothesis) would have been placed if there was no statistical difference. For this t-test, the level of significance was 0.05 with a confidence interval of 95%.

	Limestone ($\delta^{18}O$ (‰))	**Speleothem ($\delta^{18}O$ (‰))**	**Limestone ($\delta^{13}C$ (‰))**	**Speleothem ($\delta^{13}C$ (‰))**
$(\overline{x}_1 - \overline{x}_0)$	2.37	1.54	2.03	2.49
Standard error	0.93	1.47	0.39	0.31
t-test	> 0.00	> 0.00	> 0.00	> 0.00
H_0/H_a	H_a	H_a	H_a	H_a

Figure 10a and 10b show scatter plots of the speleothem and limestone tablet $\delta^{13}C$ and $\delta^{18}O$ values, respectively. Data cluster in different regions of the plot, providing a means of comparison between retrieved materials with initial compositions. The range of $\delta^{18}O$ values of the exposed tablets is larger than the range of $\delta^{13}C$ values. When all exposed tablets are considered together, both limestone and speleothem tablets show a negative $\delta^{13}C$- $\delta^{18}O$ correlation with a slope of around -3 ± 0.1 ‰.

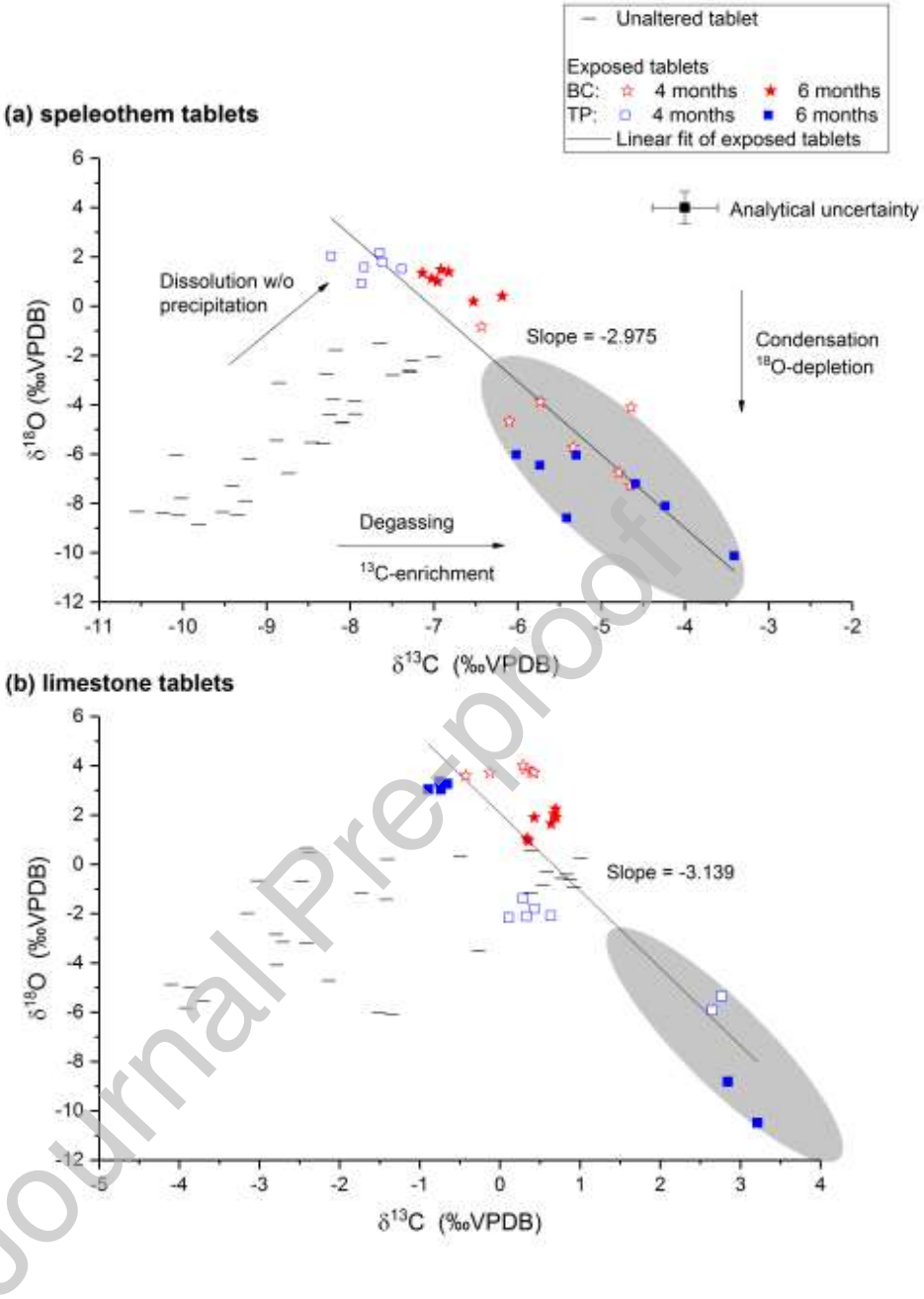

Figure 10: $\delta^{13}C$ and $\delta^{18}O$ data of unaltered and exposed speleothem (a) and limestone (b) tablets deployed in the Blanket Chamber and Tomo Passage over periods of 4 and 6 months. The ellipse identifies inferred calcite precipitates with the overprint of condensation and degassing. TP = Tomo Passage, BC = Blanket chamber.

Isotope results from both speleothem and limestone tablets for the four-month and six-month exposure periods in the Tomo Passage and Blanket Chamber, distribute along a slope of ca. -3.1 (Figure 10). Although there is some degree of consistency in

the clustering of the samples following the aforementioned negative correlation, probably the most noticeable feature is that the Tomo Passage tablets showed consistently the most offset values in the longer-term deployment for both tablet types. Oxygen and carbon isotopic signatures of the speleothem tablets generally had a greater variability (Figure 10a) compared to their more closely clustered limestone counterparts (Figure 10b).

5. Discussion

The findings of this study clearly show the strong effect of condensation corrosion on the isotope composition of exposed carbonate surfaces. Although mass loss was not conclusively demonstrated, the results point to more aggressive alteration of surfaces in the Tomo Passage, which experienced the most dynamic variations in cave microclimate between the two sites selected for isotope analysis. The results obtained here are discussed in the following sections, focusing on the mechanisms of isotopic alteration and the implications for applying stable isotope ratios in carbonates to detect episodes of condensation corrosion.

5.1 Uncertainties of the tablet method for mass comparison

Both materials used in making tablets were composed of calcite. However, the surface area in contact with the adhesive and the tensile strength of the limestone and speleothem tablets differed. The speleothem tablets were more brittle with higher porosity and exhibited the greatest weight change. The positive weight change observed for the speleothem tablets (Table 2) can be explained by different degrees of adhesive retention in the pores, which may or may not include a small quantity of wall material. In contrast, a negative weight change may result from a small quantity of rock tablet fragments being detached during the mechanical removal of the silicone. Therefore, from a gravimetric standpoint, the protocol used in the deployment of the tablets proved to be unsuccessful.

5.2 Evidence for pitting and precipitation on tablet surfaces

The potential dissolution and precipitation features (Figure 6) observed on the tablets after deployment cannot be fully confirmed by morphology alone, but could conceivably have been caused by acidic solutions during exposure in the cave. Other features which unambiguously formed during exposure could be the result of enzymatic secretion from hyphae on newly-formed calcite crystals, following deposition of airborne spores on some of the tablets [50]. *Aspergillus* sp., *Penicillium* sp. and *Cladosporium* sp. have been observed in other caves [50].

The calcite crystals that formed during the exposure periods on the tablets may have originated from groundwater percolation as there is a lack of dissolution features from where this material would have dissolved, however we cannot determine this from our isotope results (Section 5.4). Although little corrosion was observed under SEM, it does not necessarily mean it was not widespread in most samples, we suspect that the scale at which it occurred was below the capacity of the instrument.

5.3 Evidence for isotopic alteration of limestone tablets arising from condensation corrosion

The $\delta^{13}C$ values of the exposed tablets suggest a progressive enrichment of heavier isotopes during exposure, whereas the $\delta^{18}O$ values show depletion of ^{18}O. The similar standard deviations for $\delta^{13}C$ and $\delta^{18}O$ values in speleothem and limestone tablets suggest that the same processes were acting upon these materials. The t-test confirmed a statistically significant difference between the unaltered and exposed materials for the four tests.

Condensation corrosion involves the dissolution of calcite, which may or may not result in latter calcite precipitation. Hence, the $\delta^{13}C$ and $\delta^{18}O$ values reflect the distribution of carbon and oxygen isotopes between calcite and the dissolved inorganic carbon (DIC) reservoir [12,51]. Also, $\delta^{18}O$ values are inherently influenced by the initial composition of the water film on the cave walls. A large body of $\delta^{13}C$ and $\delta^{18}O$ studies has focused on understanding the environmental drivers of $\delta^{13}C$

and $\delta^{18}O$ variability [54,55], further using them as proxies for paleoclimate reconstruction using speleothems [56]. As a result, there is a well-constrained understanding of the behaviour of carbon and oxygen isotopes during precipitation of calcium carbonate. However, our review of the literature leads us to the conclusion that there is a lack of insight into carbon and oxygen fractionation during the dissolution of low-temperature carbonates. Skidmore et al. [57] studied the change in DIC $\delta^{13}C$ values during $CaCO_3$ dissolution, and other studies have reported changes in $\delta^{44/42}Ca$ [58] and $\delta^{26}Mg$ [59], during dissolution of calcite and hydromagnesite, respectively. These studies show that lighter isotopes preferentially dissolve, leaving the surface of the reacted minerals enriched in heavier isotopes. In this study, we have applied the same reasoning to the exposed tablet $\delta^{13}C$ and $\delta^{18}O$ values. Thus, exposed tablets with the highest $\delta^{18}O$ values are interpreted as occurring due to fractionation during dissolution. The tablet data with the highest $\delta^{18}O$ values also show a degree of enrichment in ^{13}C when compared to the unaltered materials. We consider this region of higher $\delta^{13}C$ and $\delta^{18}O$ values (Figure 10) to delineate the start of the condensation corrosion process (i.e. representing the carbonate dissolution end-member). If all the exposed tablet data are considered as a single set, starting at the region where the $\delta^{18}O$ values are highest and following the exposed tablet data in an increasing $\delta^{13}C$ direction, it can be observed in both Figure 10a and 10b, that there is a negative correlation between $\delta^{13}C$ and $\delta^{18}O$, spanning a consistent range of values (despite the initial composition of the tablet substrate).

In cave systems, it is normal to observe a positive correlation between $\delta^{13}C$ and $\delta^{18}O$ during the formation of speleothem calcite from drip water (Figure 10a) [12]. However, in this study, the altered surface of the tablets shows negative fractionation trends between $\delta^{13}C$ and $\delta^{18}O$, i.e. an inversion of the normal correlation.

When evaporation takes place, or when the cave air PCO_2 changes dynamically (as in the Glowworm Cave) the condensation film degasses CO_2, which favours the release of the lighter isotopologues of CO_2 into the cave atmosphere [53]. Therefore, the

$\delta^{13}C$ of DIC increases. We have assumed that the water buffering effect [52,53] minimised changes in $\delta^{18}O$ during evaporation, compared to larger $\delta^{13}C$ fractionation from degassing CO_2. As a result of these mechanisms, the tablet $\delta^{13}C$ value increases, while the $\delta^{18}O$ of the tablet surface reflects either enriched values due to dissolution of calcite, or lighter values from precipitation of calcite under non-equilibrium conditions. Where the solution becomes supersaturated, $CaCO_3$ precipitates favouring the incorporation of lighter carbon and oxygen isotopes into the calcium carbonate lattice, as found by the results of Dietzel et al. [60], Day and Henderson [61] and Hansen et al. [12]. Thus, resulting in the negative correlation between $\delta^{13}C$ and $\delta^{18}O$ found on the exposed tablets.

5.4 Detecting condensation corrosion

We suggest that the distribution of initial and final tablet $\delta^{18}O$ and $\delta^{13}C$ values milled from the upper tablet surfaces (Figure 10) provides a means of identifying dissolution of carbonate tablets (increase in both $\delta^{13}C$ and $\delta^{18}O$ values) and precipitation of calcite (more negative $\delta^{18}O$ signature with enriched $\delta^{13}C$). It is thought that during dissolution, the lighter isotopes are favoured in solution as they form weaker bonds, leaving the tablet's surface enriched in ^{18}O Oelkers *et al*. [58], Oelkers *et al.* [59]. However, if degassing occurs and $CaCO_3$ is precipitated onto the tablet's surface, we expect to observe more negative $\delta^{18}O$ values based on the Hansen *et al.* [51] study. The $\delta^{13}C$ values become more positive and this is thought to be due to the progressive removal of $^{12}CO_2$ during degassing, leaving the DIC more concentrated in ^{13}C. It is possible at lower relative humidity values (less than 80%) to get high values for both $\delta^{13}C$ and $\delta^{18}O$ as found by Deininger *et al.*, (2012). This potentially occurs because a significant enough fraction of the water reservoir is evaporated under kinetic conditions. However, this study did not record relative humidity values below 94 %. Therefore, the enrichment values observed are likely to be in response to another mechanism.

It should be noted that the depth at which condensation corrosion may affect the exposed tablets is unknown, and there is the possibility that the milled samples

contain a mixture of dissolution, precipitation and pristine isotope compositions. In this interpretive framework, although little evidence for dissolution features linking to fluid undersaturation were observed under SEM, or widespread precipitation, it does seem both processes have occurred as suggested by the $\delta^{13}C$ and $\delta^{18}O$ data in Figure 10. Most of the data appear clustered by location and exposure time, however, there are data points with a greater spread that may appear as outliers. Differences between tablets deployed in the same locations for the same duration may result from differential water film residence times due to small variations in the inclination of the cave's walls and ceilings thereby causing the condensate to remain on the tablet surface, or flow away. There is no way to retrospectively make this determination, but this seems logically consistent.

The $\delta^{13}C$ and $\delta^{18}O$ data (Figure 10) showed different isotopic responses in the tablets over the four- and six-month periods of exposure. During the first four months in the Blanket Chamber, it appears that there was corrosion without subsequent precipitation on the limestone tablets (Figure 10b), as these points have a higher $\delta^{18}O$ compositions. However, two months later, it appears that there was precipitation on the limestone tablets as the $\delta^{18}O$ values were lower by ~2‰. However, this trend was inverted in the speleothem samples, which showed evidence of greater precipitation in the first four months (lower $\delta^{18}O$, higher $\delta^{13}C$).

In the case of the Tomo Passage, during the initial four months, the $\delta^{18}O$ values of speleothem tablets (Figure 10a) were high, which suggests that dissolution was taking place and the DIC was largely removed by flow in the condensation water. In the latter two months, there is evidence for corrosion and precipitation on the speleothem tablets (lower $\delta^{18}O$, higher $\delta^{13}C$). Although the data from the Tomo Passage may appear to be contradictory (Figure 10a), the action of dissolution (predominant process inferred from the 4-month deployments) and precipitation (predominant process inferred from the 6-month deployments) on the speleothem surfaces, need not have been mutually exclusive. For example, a period of dissolution could be overprinted by subsequent precipitation in the two months following retrieval of the 4-month tablets. These differences may also arise due to

differences in the orientation of tablets or other factors that are outside of the scope of the present study.

Overall, the findings of this study point to the potential for the isotopic composition of speleothem surfaces to be modified by condensation corrosion, given sufficient time. Indeed, the negative correlation between $\delta^{13}C$ and $\delta^{18}O$ in exposed surfaces observed in this study is in agreement with the antipathetic $\delta^{13}C$ and $\delta^{18}O$ pattern observed at high resolution through growth hiatuses in Siberian stalagmites [62]. Researchers working in speleothem paleoclimatology may, therefore, be interested in determining whether hiatuses in speleothem growth are overprinted by condensation corrosion processes based on $\delta^{13}C$ and $\delta^{18}O$ values.

6. Conclusion

The use of $\delta^{13}C$ and $\delta^{18}O$ values from the tablet method provides a novel approach to detecting condensation corrosion. Carbon and oxygen isotope ratios appear to be fractionated as a result of both dissolution (small, positive enrichment), and precipitation of $CaCO_3$ associated with the condensation and evaporation of thin water films (depletion of $\delta^{18}O$, enrichment of $\delta^{13}C$). Although this method appears to be sensitive to the operation of condensation corrosion, it does not permit estimates of the magnitude or duration of the corrosion episodes, which will vary depending on the cave's relative humidity, partial CO_2 pressure and temperature gradient.

In Glowworm Cave, the chambers and passages likely respond independently of each other, resulting in distinct isotopic differences. The differences between chambers may have been caused by a combination of seasonal effects, direct ventilation by cave management and passing groups of tourists. But further work is needed to evaluate intra-cavern differences with respect to the particular microclimate.

Finally, the results of this study may have greater relevance to researchers studying the paleoclimatic significance of stable oxygen and carbon isotope variations in

speleothems and may provide a framework for identifying past episodes of condensation corrosion, punctuating otherwise continuous carbonate deposition.

7. Acknowledgements

We thank Tourism Holdings Ltd who manage the Glowworm Cave for funded this study. We are grateful to Carl Fisher, Callum Styles, Travis Cross and Shannon Corkill for helping with fieldwork and providing monitoring data from Glowworm Cave.

This project would have not been possible without technical support from Helen Turner (SEM analysis), Kathleen Dabell and Anjana Rajendram (isotope measurements), Dr Joanne Kelly (fungi identification), Annette Rodgers and Kirsty Vincent (sample preparation for XRF and XRD analysis) and Renat Radonsinsky (training with the rock preparation).

We are also grateful to three anonymous reviewers, whose comments greatly improved the quality of this manuscript.

Competing interests' statement

The authors have no competing interests to declare.

References

[1] C.R. de Freitas, A.A. Schmekal, Condensation as a microclimate process: measurements, numerical simulation and prediction in the Glowworm Cave, New Zealand, Int. J. Climatol., 2003, 23, 557-575. https://doi.org/10.1002/joc.898.

[2] D. Ford, P. Williams, Karst and Geomorphology, Rev. ed., John Wiley & Sons, Chichester, England, 2007.

[3] Y.V. Dublyansky, C. Spotl, Condensation-corrosion speleogenesis above a carbonate-saturated aquifer: Devils Hole Ridge, Nevada, Geomorphology, 2015, 229, 17-29. https://doi.org/10.1016/j.geomorph.2014.03.019.

[4] V.N. Dublyansky, Y.V. Dublyansky, The problem of condensation in karst studies, J. Caves Karst Stud., 1998, 60, 3-17.

[5] F. Gázquez, J.M. Calaforra, N.P. Evans, D.A. Hodell, Using stable isotopes (δ17O, δ18O and δD) of gypsum hydration water to ascertain the role of water condensation in the formation of subaerial gypsum speleothems, Chem. Geol., 2017, 452, 34-46. https://doi.org/10.1016/j.chemgeo.2017.01.021.

[6] O. Carville, 2017, 5 May. The Great Tourism Squeeze: Small town tourist destinations buckle under weight of New Zealand's tourism boom, The New Zealand Herald. https://www.nzherald.co.nz/nz/news/article.cfm?c_id=1&objectid=11828398 (accessed May 2020).

[7] D. Dragovich, J. Grose, Impact of tourists on carbon dioxide levels at Jenolan Caves, Australia: an examination of microclimatic constraints on tourist cave management, Geoforum, 1990, 21, 111-120. https://doi.org/10.1016/0016-7185(90)90009-U.

[8] K. Krklec, D. Dominguez-Villar, R.M. Carrasco, J. Pedraza, Current denundation rates in dolostone karst from central Spain: Implications for the formation of unroofed caves, Geomorphology, 2016, 264, 1-11. https://doi.org/10.1016/j.geomorph.2016.04.007.

[9] N.M. Miedema, 2009. Non-Anthropogenic Sources of Carbon Dioxide in the Glowworm Cave, Waitomo. MSc thesis, University of Waikato, Hamilton, New Zealand.

[10] M.J. Gillies, 2011. Microclimate and Effects of Visitor Numbers and Ventilation on Carbon Dioxide Concentration in the Waitomo Glowworm Cave, New Zealand. BSc Hon. thesis, University of Auckland, Auckland, New Zealand.

[11] W. Dreybrodt, F. Gabrovšek, M. Perne, Condensation Corrosion: A theoretical approach, Acta Carsologica, 2005, 34, 317-348. https://doi.org/10.3986/ac.v34i2.262.

[12] M. Hansen, D. Scholz, B.R. Schöne, C. Spötl, Simulating speleothem growth in the laboratory: Determination of stable isotope fraction ($\delta^{13}C$ and $\delta^{18}O$) between H_2O, DIC and $CaCO_3$, Chem. Geol., 2019, 509, 20-44. https://doi.org/10.1016/j.chemgeo.2018.12.012.

[13] C.R. de Freitas, R.N. Littlejohn, Cave climate: assessment of heat and moisture exchange, J. Climatol., 1987, 7, 553-569. https://doi.org/10.1002/joc.3370070604.

[14] G. Badino, Clouds in caves, Speleogenesis and Evolution of Karst Aquifers, 2004, 2, 1-8.

[15] J. Wallace, P. Hobbs, Atmospheric science: An introduction survey, 2nd ed., Elsevier USA, Boston, 2006.

[16] C.R. de Freitas, A. Schmekal, Studies of condensation/evaporation processes in the Glowworm Cave, New Zealand, Int. J. Speleol., 2006, 35, 75-81. http://dx.doi.org/10.5038/1827-806X.35.2.3.

[17] R.D. Deshpande, A.S. Maurya, B. Kumar, A. Sarkar, S.K. Gupta, Kinetic fractionation of water isotopes during liquid condensation under super-saturated condition, Geochim. Cosmochim. Acta, 2013, 100. https://doi.org/10.1016/j.gca.2012.10.009.

[18] S.-T. Kim, T.B. Coplen, J. Horita, Normalization of stable isotope data for carbonate minerals: Implementation of IUPAC guidelines, Geochim. Cosmochim. Acta, 2015, 158, 276-289. https://doi.org/10.1016/j.gca.2015.02.011.

[19] S. Sánchez-Moral, V. Soler, J.C. Cañaveras, E. Sanz-Rubio, R. Van Grieken, K. Gysels, Inorganic deterioration affection the Altamira Cave, N Spain: quantitative approach to wall-corrosion (solutional etching) processes induced by visitors, Sci. Total Environ., 1999, 243, 67-84. https://doi.org/10.1016/S0048-9697(99)00348-4.

[20] C. Hendy, The isotopic geochemistry of speleothems—I. The calculation of the effects of different modes of formation on the isotopic composition of speleothems and their applicability as palaeoclimatic indicators, Geochim. Cosmochim. Acta, 1971, 35, 801-824. https://doi.org/10.1016/0016-7037(71)90127-X.

[21] A.A. Schmekal, C.R. de Freitas, 2001. Condensation in Glow-worm Cave, Waitomo, New Zealand. Department of Conservation Science Internal Series 15, Wellington, New Zealand. 11p.

[22] A.S. Auler, P.L. Smart, Rates of condensation corrosion in speleothems of semi-arid northeastern Brazil, Speleogenesis and Evolution of Karst Aquifers, 2004, 2, 1-2.

[23] S. Galdenzi, Corrosion of limestone tablets in sulfidic ground-water: measurements and speleogenetic implications, Int. J. Speleol., 2012, 41, 3. http://dx.doi.org/10.5038/1827-806X.41.2.3.

[24] M. Vattano, P. Audra, F. Benvenuto, J.Y. Bigot, J. De Waele, E. Galli, G. Madonia, J. Nobécourt, Hypogenic caves of Sicily (southern Italy), in: Proceedings of the 16th international congress of speleology, Vol. 3, 2013, pp. 144-149.

[25] F. Bourges, P. Genthon, D. Genty, M. Lorblanchet, E. Maunduit, D. D'Hulst, Conservation of prehistoric caves and stability of their inner climate: lessons from Chauvet and other French caves, Sci. Total Environ., 2014, 493, 79-91. https://doi.org/10.1016/j.scitotenv.2014.05.137.

[26] P. Audra, F. Hoblea, J.Y. Bigot, J.C. Nobécourt, The Role of Condensation Corrosion in Thermal Speleogenesis. Study of a Hypogenic Cave in Aix-les-Bains, France, Acta Carsologica, 2007, 36. https://doi.org/10.3986/ac.v36i2.186.

[27] P. Forti, S. Galdezi, S.M. Sarbu, The hypogenic caves: a powerful tool for the study of seeps and their environmental effects, Cont. Shelf Res., 2002, 22, 2373-2386. https://doi.org/10.1016/S0278-4343(02)00062-6.

[28] F. Gázquez, J.M. Calaforrab, P. Fortic, J. De Waelec, L. Sannad, The role of condensation in the evolution of dissolutional forms in gypsum caves: Study case in the karst of Sorbas (SE Spain), Geomorphology, 2015, 229, 100-111. https://doi.org/10.1016/j.geomorph.2014.07.006.

[29] G.A. Caddeo, L.B. Railsback, J. De Waele, F. Frau, Stable isotope data as constraints on models for the origin of coralloid and massive speleothems: the interplay of substrate, water supply, degassing, and evaporation, Sediment. Geol., 2015, 318, 130-141. https://doi.org/10.1016/j.sedgeo.2014.12.008.

[30] Z. Sharp, Principles of stable isotope geochemistry, Pearson/Prentice Hall, Upper Saddle River, N.J., 2007.

[31] J. Galewsky, H.C. Steen-Larsen, R.D. Field, J. Worden, C. Risi, M. Schneider, Stable isotopes in atmospheric water vapor and applications to the hydrologic cycle, Rev. Geophys., 2016, 54, 809-865. https://doi.org/10.1002/2015RG000512.

[32] T.W. Horton, W.F. Defliese, A.K. Tripati, C. Oze, Evaporation induced ^{18}O and ^{13}C enrichment in lake systems: A global perspective on hydrologic balance effects, Quat. Sci. Rev., 2016, 131, 365-379. https://doi.org/10.1016/j.quascirev.2015.06.030.

[33] W. Dreybrodt, M. Hansen, D. Scholz, Processes affecting the stable isotope composition of calcite during precipitation in the surface of stalagmites: Laboratory experiments investigating the isotope exchange between DIC in the solution layer on top of a speleothem and the CO2 of the cave atmosphere., Geochim. Cosmochim. Acta, 2016, 174, 247-262. https://doi.org/10.1016/j.gca.2015.11.012.

[34] D.F. Ufnar, D.R. Gröcke, P.A. Beddows, Assessing pedogenic calcite stable-isotope values: Can positive linear covariant trends be used to quantify palaeo-evaporation rates?, Chem. Geol., 2008, 256, 46-51. https://doi.org/10.1016/j.chemgeo.2008.07.022.

[35] D.M. Tremaine, P.N. Froelich, Y. Wang, Speleothem calcite farmed *in situ*: Modern calibration of $\delta^{18}O$ and $\delta^{13}C$ paleoclimate proxies in a continuously-monitored natural cave system, Geochim. Cosmochim. Acta, 2011, 75, 4929-4950. https://doi.org/10.1016/j.gca.2011.06.005.

[36] W. Dreybrodt, Evolution of the isotopic composition of carbon ad oxygen in a calcite precipitating H_2O–CO_2–$CaCO_3$ solution and the related isotopic composition of calcite in stalagmites, Geochim. Cosmochim. Acta, 2008, 72, 4712-4724. https://doi.org/10.1016/j.gca.2008.07.022.

[37] M. Deininger, J. Fohlmeister, D. Scholz, A. Mangini, Isotope disequilibrium effects: The influence of evaporation and ventilation effects on the carbon and oxygen isotope composition of speleothems – A model approach., Geochim. Cosmochim. Acta, 2012, 96, 57-79. https://doi.org/10.1016/j.gca.2012.08.013.

[38] Institute of Geological & Nuclear Sciences, S.W. Edbrooke, Geology of the Waikato area, Vol. 1, Institute of Geological & Nuclear Sciences, 2005.

[39] C.S. Nelson, 1973. Stratigraphy and sedimentology of the Te Kuiti Group in Waitomo County, South Auckland. PhD thesis, University of Auckland, Auckland, New Zealand.

[40] A.S. Anastas, R.W. Dalrymple, N.P. James, C.S. Nelson, Lithofacies and dynamics of a cool-water carbonate seaway: mid-Tertiary, Te Kuiti Group, New Zealand, Geol. Soc. Spec. Publ., 2006, 255, 245-268. https://doi.org/10.1144/GSL.SP.2006.255.01.15.

[41] S.M. Mentzer, Micro XRF, Archaeological soil and sediment micromorphology, 2017, 431-440.

[42] A.R. Pearson, A. Hartland, S. Frisia, B.R. Fox, Formation of calcite in the presence of dissolved organic matter: Partitioning, fabrics and fluorescence., Chem. Geol., 2020, 539, 119492. https://doi.org/10.1016/j.chemgeo.2020.119492.

[43] S.L.L. Barker, G.M. Dipple, F. Dong, S. Baer, Use of Laser Spectrometry To Measure the 13C/12C and 18O/16O Compositions of Carbonate Minerals, Anal. Chem., 2011, 83, 2220-2226. https://doi.org/10.1021/ac103111y.

[44] A. Beinlich, S.L. Barker, G.M. Dipple, M. Gupta, D.S. Baer, Stable isotope (δ13C, δ18O) analysis of sulfide-bearing carbonate samples using laser absorption spectrometry., Econ. Geol., 2017, 112, 693-700. https://doi.org/10.2113/econgeo.112.3.693.

[45] D. Freedman, R. Pisani, R. Purves, Statistics, W.W. Norton & Company, New York, NY, 2007.

[46] J.M. Utts, Seeing Through Statistics, 4th ed., Cengage Learning, Stamford, CT, 2015.

[47] K.F. Weaver, V. Morales, S.L. Dunn, K. Godde, P.F. Weaver, t-Test, in: An Introduction to Statitical Analysis in Research: With Applications in the Biological and Life Sciences, John Wiley & Sons, Hoboken, NJ, 2017, pp. 195-225.

[48] J. Fohlmeister, N.R.G. Voarintsoac, F.A. Lechleitner, M. Boyd, S. Brandtstätter, M.J. Jacobson, J.L. Oster, Main controls on the stable carbon isotope composition of speleothems

Geochim. Cosmochim. Acta, 2020, 279, 67-87. https://doi.org/10.1016/j.gca.2020.03.042.

[49] C. Nava-Fernandez, A. Hartland, F. Gázquez, O. Kwiecien, N. Marwan, B. Fox, J. Hellstrom, A. Pearson, B. Ward, A. French, D.A. Hodell, A. Immenhauser, S.F.M. Breitenbach, Pacific climate reflected in Waipuna Cave dripwater hydrochemistry, Hydrol. Earth Syst. Sci. Discuss., 2020. http://doi.org/10.5194/hess-2019-647.

[50] E. Porca, V. Jurado, P.M. Martin-Snachez, B. Hermosin, F. Bastian, C. Alabouvette, C. Saiz-Jimenez, Aerobiology: An ecological indiator for early detection and control of fungal outbreaks in caves, Ecol. Indic., 2011, 11, 1594-1598. https://doi.org/10.1016/j.ecolind.2011.04.003.

[51] M. Hansen, D. Scholz, M.-L. Froeshmann, B.R. Schöne, C. Spötl, Carbon isotope exchange between gaseous CO2 and thin solution films: Artificial cave experiments and a complete diffusion-reaction model, Geochim. Cosmochim. Acta, 2017, 211, 28-47. https://doi.org/10.1016/j.gca.2017.05.005.

[52] D. Scholz, C. Mühlinghaus, A. Mangini, Modelling $\delta^{13}C$ and $\delta^{18}O$ in the solution layer on stalagmite surfaces, Geochim. Cosmochim. Acta, 2009, 73, 2592-2602. https://doi.org/10.1016/j.gca.2009.02.015.

[53] C. Mühlinghaus, D. Scholz, A. Mangini, Modelling fractionation of stable isotopes in stalagmites, Geochim. Cosmochim. Acta, 2009, 73, 7275-7289. https://doi.org/10.1016/j.gca.2009.09.010.

[54] S.-T. Kim, J.R. O'Neil, Equilibrium and nonequilibrium oxygen isotope effects in synthetic carbonates, Geochim. Cosmochim. Acta, 1997, 61, 3461-3475. https://doi.org/10.1016/S0016-7037(97)00169-5.

[55] T.B. Coplen, Calibration of the calcite–water oxygen-isotope geothermometer at DEvils Hole, Nevada, a natural laboratory, Geochim. Cosmochim. Acta, 2007, 71, 3948-3957. https://doi.org/10.1016/j.gca.2007.05.028.

[56] F. McDermott, Palaeo-climate reconstruction from stable isotope variation in speleothems: a review, Quat. Sci. Rev., 2004, 23, 901-918. https://doi.org/10.1016/j.quascirev.2003.06.021.

[57] M. Skidmore, M. Sharp, M. Tranter, Kinetic isotopic fractionation during carbonate dissolution in laboratory experiments: implicatinos for detection of microbial CO2 sigantures using δ13C-DIC., Geochim. Cosmochim. Acta, 2004, 68, 4309-4317. https://doi.org/10.1016/j.gca.2003.09.024.

[58] E.H. Oelkers, P.A.P. von Strandmann, V. Mavromatis, The rapid resetting of the Ca isotopic signatures of calcite at ambient temperature during its congruent dissolution, precipitation, and at equilibrium, Chem. Geol., 2019, 512, 1-10. https://doi.org/10.1016/j.chemgeo.2019.02.035.

[59] E.H. Oelkers, U.N. Berninger, A. Pérez-Fernàndez, J. Chmeleff, V. Mavromatis, The temporal evolution of magnesium isotope fractionation during hydromagnesite dissolution, precipitation, and at equilibrium, Geochim. Cosmochim. Acta, 2018, 226, 36-49. https://doi.org/10.1016/j.gca.2017.11.004.

[60] M. Dietzel, J. Tang, A. Leis, S.J. Köhler, Oxygen isotopic fractionation during inorganic calcite precipitation — Effects of temperature, precipiation rate and pH, Chem. Geol., 2009, 268, 107-115. https://doi.org/10.1016/j.chemgeo.2009.07.015.

[61] C.C. Day, G.M. Henderson, Oxygen isotopes in calcite grown under cave-analogue conditions, Geochim. Cosmochim. Acta, 2011, 75, 3956-3972. https://doi.org/10.1016/j.gca.2011.04.026.

[62] F.A. Lechleitner, A.J. Mason, S.F.M. Breitenbach, A. Vaks, N. Haghipour, G.M. Henderson, Permafrost-related hiatuses in stalagmite: Evaluating the potential for reconstruction of carbon cycle dynamics, Quat. Geochronol., 2020, 56, 101037. https://doi.org/10.1016/j.quageo.2019.101037.